EurJIC
European Journal of Inorganic Chemistry

Research Article
doi.org/10.1002/ejic.202200482

Chemistry Europe
European Chemical Societies Publishing

www.eurjic.org

VIP *Very Important Paper*

Lewis Superacidic Divalent Bis(*m*-terphenyl)element Cations $[(2,6\text{-}Mes_2C_6H_3)_2E]^+$ of Group 13 Revisited and Extended (E=B, Al, Ga, In, Tl)

Daniel Duvinage,[a] Lorraine A. Malaspina,[b] Simon Grabowsky,*[b] Stefan Mebs,*[c] and Jens Beckmann*[a]

Dedicated to Professor Klaus Jurkschat on the occasion of his 70th birthday.

In a combined experimental and computational study, the molecular and electronic structures of the divalent bis(*m*-terphenyl)element cations $[(2,6\text{-}Mes_2C_6H_3)_2E]^+$ of group 13 (**1**, E=B; **2**, E=Al; **3**, E=Ga; **4**, E=In; **5**, E=Tl) were investigated. The preparation and characterization of **2**, **3** and **5** were previously reported by Wehmschulte's (*Organometallics* **2004**, 23, 1965–1967; *J. Am. Chem. Soc.* **2003**, *125*, 1470–1471) and our groups (*Organometallics* **2009**, *28*, 6893–6901). The indinium ion **4** was prepared and fully characterized for the first time. Attempts to prepare the borinium ion **1** by fluoride or hydride abstraction were unsuccessful. The electronic structures of **1**–**5** and the stabilization by the bulky *m*-terphenyl substituents were analyzed using quantum chemical calculations and compared to the divalent bis(*m*-terphenyl)pnictogenium ions $[(2,6\text{-}Mes_2C_6H_3)_2E]^+$ of group 15 (**6**, E=P; **7**, E=As; **8**, E=Sb; **9**, E=Bi) previously investigated by our group (*Angew. Chem. Int. Ed.* **2018**, *57*, 10080–10084). The calculated fluoride ion affinities (FIA) of **1**–**9** are higher than that of SbF_5, which classifies them as Lewis superacids.

Introduction

Borinium ions[1] and their heavier group 13 analogs[2] have received tremendous interest over the years, but the first truly two-coordinate borinium ion, $[Mes_2B]^+$, was only recently reported by Shoji *et al.*[3] The interest in these four-valence-electron (4 VE) species stems from their high Lewis acidity and applications in bond activation chemistry and catalysis deriving therefrom.[1]

The present work revisits and extends a series of bulky bis(*m*-terphenyl) element cations $[(2,6\text{-}Mes_2C_6H_3)_2E]^+$ (**1**, E=B; **2**, E=Al;[4] **3**, E=Ga;[5] **4**, E=In; **5**, E=Tl[6]), for which three examples were already reported by Wehmschulte *et al.*[4,5] and our group.[6] Here we describe the analogous $[(2,6\text{-}Mes_2C_6H_3)_2In]^+$ (**4**), which represents the first donor-free, two-coordinate indinium ion. By contrast, all previously known related indenium cations, such as $[(Me_3SiCH_2)_2In(THF)_3]^+$ and $[Mes_2In]^+[BF_4]^-$, possess saturated hypercoordinate indium atoms due to solvation or ion pairing.[7] We also report on our failed attempts to prepare the related borinium ion $[(2,6\text{-}Mes_2C_6H_3)_2B]^+$ (**1**) by fluoride and hydride abstraction.[3]

Complementing the experimental results, the electronic structures of **1**–**5** were investigated by density functional theory (DFT) calculations and real space bond indicator (RSBI) analyses. RSBIs comprise bond topology according to the Atoms-In-Molecules (AIM)[8] theory, intramolecular contact patches according to the noncovalent interactions (NCI)[9] index, and bonding and lone-pair basins according to the electron localizability indicator (ELI–D).[10] The results of group 13 are compared to a complementary series of group 15 cations $[(2,6\text{-}Mes_2C_6H_3)_2E]^+$ (**6**, E=P; **7**, E=As;[11] **8**, E=Sb; **9**, E=Bi[12]), possessing six valence electrons (6 VE) which were either assigned as transient species in fluoride abstraction reactions[11] or isolated and fully characterized by us previously.[12]

Results and Discussion

Attempted preparation of the borinium ion $[(2,6\text{-}Mes_2C_6H_3)_2B]^+$ (1)

The reaction of *m*-terphenyllithium, $2,6\text{-}Mes_2C_6H_3Li$,[13] with an excess of boron trifluoride etherate, $BF_3{\cdot}OEt_2$, provided the mono-substituted product $2,6\text{-}Mes_2C_6H_3BF_2$ (**10**) in 66% yield (Scheme 1). After isolation of **10**, the reaction with $2,6\text{-}Mes_2C_6H_3Li$ afforded the di-substituted product $(2,6\text{-}Mes_2C_6H_3)_2BF$ (**11**) in 82% yield (Scheme 1). Efforts were made

[a] D. Duvinage, Prof. Dr. J. Beckmann
Institut für Anorganische Chemie und Kristallographie,
Universität Bremen,
Leobener Straße 7, 28359 Bremen, Germany
E-mail: j.beckmann@uni-bremen.de
[b] Dr. L. A. Malaspina, PD Dr. S. Grabowsky
Departement für Chemie, Biochemie und Pharmazie,
Universität Bern,
Freiestrasse 3, 3012 Bern, Switzerland
E-mail: simon.grabowsky@unibe.ch
[c] Dr. S. Mebs
Institut für Experimentalphysik, Freie Universität Berlin,
Arnimallee 14, 14195 Berlin, Germany
E-mail: stefan.mebs@fu-berlin.de

Supporting information for this article is available on the WWW under https://doi.org/10.1002/ejic.202200482

Research Article
doi.org/10.1002/ejic.202200482

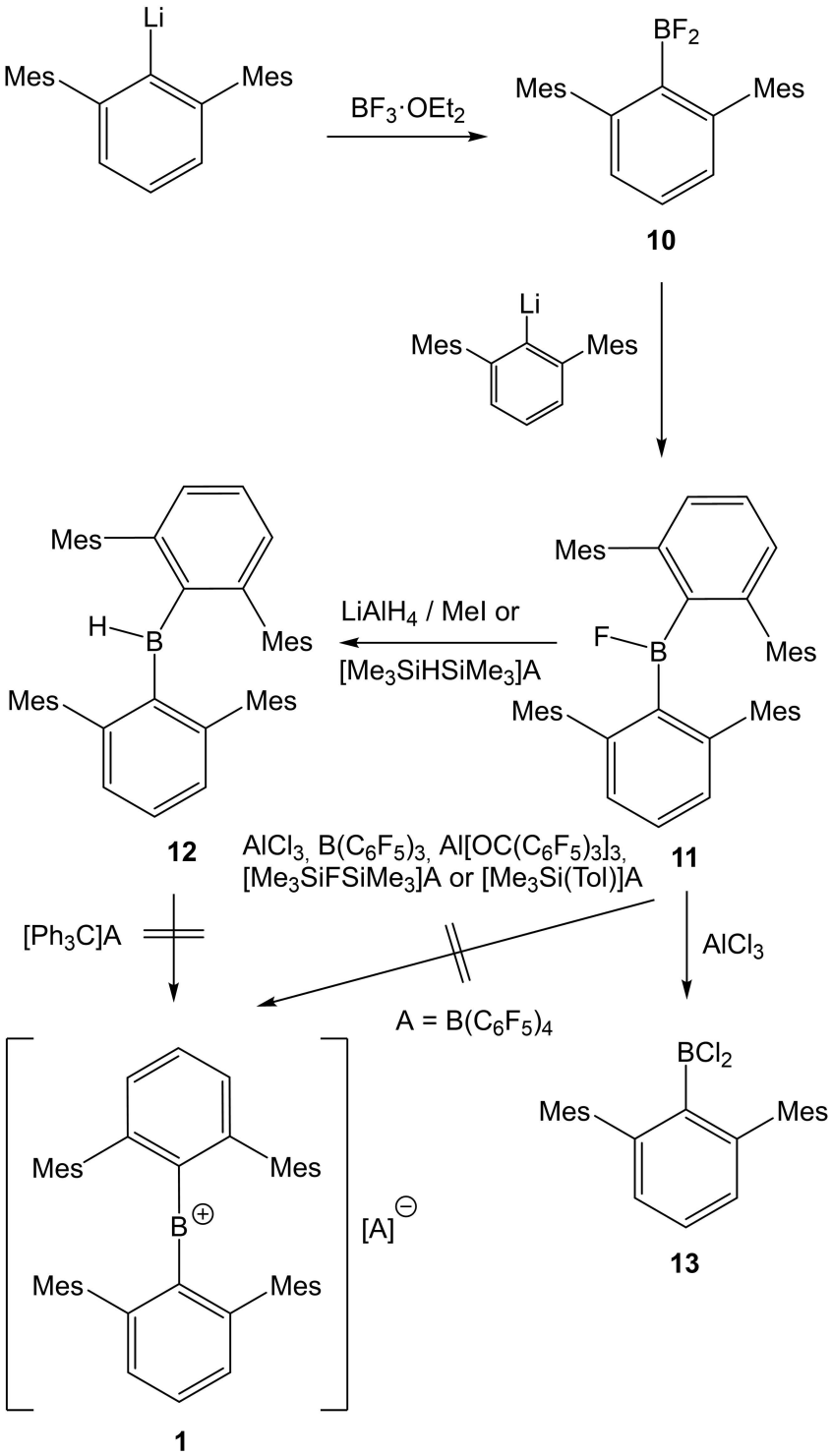

Scheme 1. Synthesis of mono- and di-substituted *m*-terphenyl boranes **10**, **11** and **12** and attempted preparation of the borinium ion **1**.

to prepare **11** in a one-pot procedure; however, it was noted that the second equivalent of 2,6-$Mes_2C_6H_3Li$ attacks the ether molecule under these Lewis acidic conditions. Both *m*-terphenylboron fluorides could be readily distinguished by heteronuclear NMR spectroscopy. The ^{11}B NMR spectra (CD_2Cl_2) of **10** and **11** show broad signals at $\delta = 25.3$ ($W_{1/2} = 1500$ Hz) and 51.4 ppm ($W_{1/2} = 1600$ Hz), respectively. The ^{19}F NMR spectra (CD_2Cl_2) of **10** and **11** reveal very different signals at $\delta = -70.9$ and 17.5 ppm. The reduction of **11** with $LiAlH_4$ (after workup with MeI) produced the corresponding bis(*m*-terphenyl)boron hydride (2,6-$Mes_2C_6H_3)_2BH$ (**12**) in 96% yield (Scheme 1). The ^{11}B NMR spectrum (CD_2Cl_2) of **12** shows a broad signal at $\delta =$

Research Article
doi.org/10.1002/ejic.202200482

74.3 ppm. The IR spectrum (ATR, neat) of **12** exhibits a peak at $\tilde{\nu} = 2580\ cm^{-1}$, which was assigned to the terminal B–H stretching vibration.

The bis(*m*-terphenyl)boranes **11** and **12** were used for the attempted preparation of the borinium ion **1**. The attempted fluoride abstraction of (2,6-$Mes_2C_6H_3)_2BF$ (**11**) with $AlCl_3$ gave rise to mixture of products, from which only the previously known mono-substituted product 2,6-$Mes_2C_6H_3BCl_2$ (**13**)[14] was isolated by crystallization in low yields (Scheme 1). In the remaining dark oil, only the parent *m*-terphenyl ligand 2,6-$Mes_2C_6H_4$ was identified. The reaction of **11** with the milder Lewis acid $EtAlCl_2$ occurred at slower pace, but it also gave multiple products. No reactivity was observed between **11** and the bulkier Lewis acids $B(C_6F_5)_3$[15] and $Al[OC(C_6F_5)_3]_3$.[16] The reaction of **11** with the disguised silylium ion $[Me_3Si–H–SiMe_3][B(C_6F_5)_4]$[17] proceeded with a smooth H/F exchange and afforded (2,6-$Mes_2C_6H_3)_2BH$ (**12**) and the previously known fluorine-bridged species $[Me_3Si–F–SiMe_3][B(C_6F_5)_4]$.[18] With $[Me_3Si{\cdot}toluene][B(C_6F_5)_4]$, prepared *in situ* from $[Me_3Si–H–SiMe_3][B(C_6F_5)_4]$ and toluene,[17] multiple signals were observed by ^{11}B and ^{19}F NMR spectroscopy, which tentatively suggests that the bis(*m*-terphenyl)borane moiety as well as the borate anion had degraded. Similar observations were made by Wehmschulte[19] and Power.[14] The attempted hydride abstraction of (2,6-$Mes_2C_6H_3)_2BH$ (**12**) with the trityl salt $[Ph_3C][B(C_6F_5)_4]$[20] gave no reaction (Scheme 1).

The molecular structures of **10** and **13** are shown in Figure 1. Selected bond parameters of the series 2,6-$Mes_2C_6H_3BX_2$ (**10**, X=F; **13**, X=Cl and X=Br[14]) are collected in Table 1. The spatial arrangements of **10** and **13**, like the previously studied 2,6-$Mes_2C_6H_3BBr_2$, are slightly distorted trigonal planar.[14] As anticipated, the B–X bond length increases from **10** (1.307(2), 1.314(2) Å for X=F) to **13** (1.750(1) Å for X=Cl) and 2,6-$Mes_2C_6H_3BBr_2$ (1.903(1) Å for X=Br), whereas the other bond parameters (B–C bond lengths, X–B–X, X–B–C bond angles) show little variance.

The molecular structures of **11** and **12** are shown in Figure 2. Selected bond parameters of the series (2,6-$Mes_2C_6H_3)_2BX$ (**11**, X=F; **12**, X=H) and Mes_2BF[21] are collected in Table 2. Unlike Mes_2BF, the geometries of **11** and **12** strongly deviate from an ideal trigonal planar arrangement. Due to the repulsion of the bulky *m*-terphenyl substituents, the C–B–C bond angles of **11** (142.0(1)°) and **12** (136.6(1)°) are dramatically enlarged as compared to that of Mes_2BF (125.4(1)°). In turn, the X–B–C bond angles of **11** (107.1(1) and 110.9(1)°) and **12** (111.7(1)°) are significantly compressed in comparison to that of Mes_2BF[21] (116.8(1) and 117.8(1)°). The B–F bond lengths of **11** and Mes_2BF (1.339(2) Å) are identical within the experimental error and slightly longer than in **10** (1.307(2) and 1.314(2) Å). The B–C bond length increases from Mes_2BF[21] (1.568(2) and 1.570(2) Å) to **12** (1.573(1) Å) and **11** (1.586(2) and 1.599(2) Å) reflecting the bulk of the three substituents. We speculate that the slight elongation of the B–C bonds in **11** might be the reason why the cleavage of the second *m*-terphenyl substituent occurs in the reaction with $AlCl_3$ (see above).

Table 1. Selected bond lengths in Å and angles in ° of **10**, **13** and 2,6-$Mes_2C_6H_3BBr_2$.[14]

	10 (X=F)	**13** (X=Cl)	2,6-$Mes_2C_6H_3BBr_2$
B–X	1.307(2), 1.314(2)	1.750(1)[a]	1.903(1)[a]
B–C	1.560(2)	1.558(2)	1.565(1)
X–B–X	115.4(1)	116.4(1)	116.3(1)
X–B–C	122.2(1), 122.4(1)	121.8(1)	121.8(1)

[a] The two chlorine and two bromine atoms are crystallographically equivalent.

Table 2. Selected bond lengths in Å and angles in ° of **11**, **12** and Mes_2BF.[21]

	11 (X=F)	**12** (X=H)	Mes_2BF
B–X	1.339(2)	1.203(4)	1.339(2)
B–C	1.586(2), 1.599(2)	1.573(1)	1.568(2), 1.570(2)
X–B–C	107.1(1), 110.9(1)	111.7(1)	116.8(1), 117.8(1)
C–B–C	142.0(1)	136.6(1)	125.4(1)

The structure of **12** was subject to a Hirshfeld atom refinement (HAR),[22] which allows the precise and accurate determination of E–H bonds from X-ray data.[23] The B–H bond length of **12** (1.203(4) Å) can be compared to the other four existing HAR-refined terminal B–H bond length values in the literature, whereas neutron-diffraction references are missing in the literature. The B–H bond length in **12** is identical within the experimental error with those of *closo*-borane $(NH_4)_2[B_6H_6]$[24] and the terminal ones in the copper(I) complex $[(Ph_3P)_2Cu][BH_4]$[23] despite the different coordination numbers of the boron atoms. In contrast, the terminal B–H bonds in diborane $(BH_3)_2$[23] and the cobalt(II) complex $Co(Bm^{Me})_2$ (Bm^{Me} = bis(2-mercapto-1-methylimidazolyl)borate)[25] are significantly shorter at 1.170(7)/1.168(6) Å and 1.174(13) Å, respectively.

Figure 1. Molecular structures of the mono-substituted *m*-terphenylboron difluoride **10** and dichloride **13** showing 50% probability ellipsoids.

Research Article
doi.org/10.1002/ejic.202200482

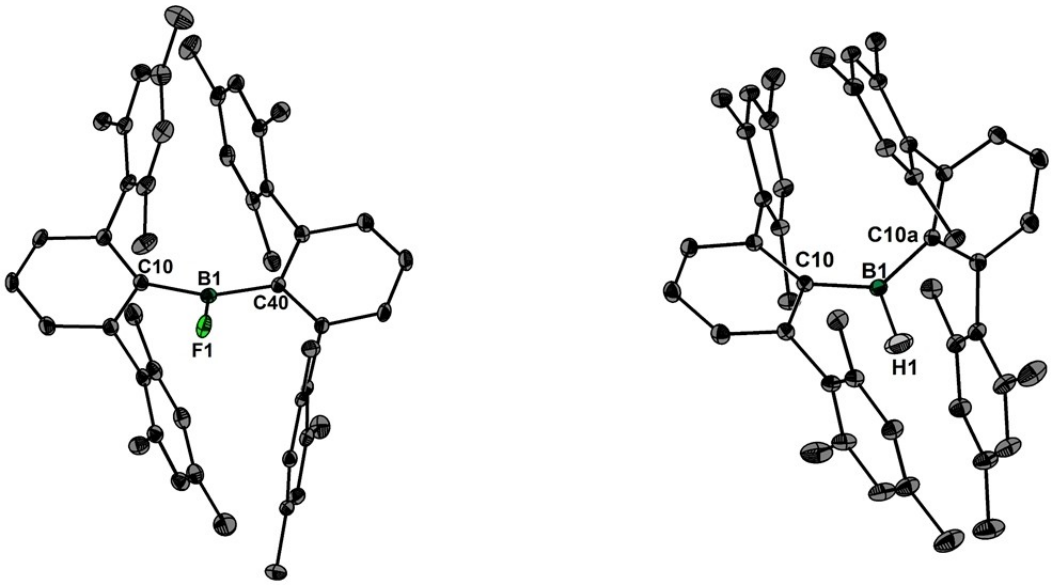

Figure 2. Molecular structure of the di-substituted *m*-terphenylboron fluoride **11** and hydride **12** (derived from Hirshfeld atom refinement (HAR)) showing 50% probability ellipsoids.

Preparation of the indinium cation 4

The indinium cation **4** was synthesized by bromide abstraction from (2,6-$Mes_2C_6H_3)_2InBr$[26] using $K[B(C_6F_5)]_4$[27] and obtained as orange crystals in 91% yield (Scheme 2). In solution, **4** reveals the typical set of *m*-terphenyl signals by ^1H NMR spectroscopy. In ^{13}C NMR spectroscopy, the influence of the positive charge is best visible in the shift of the *ipso* carbon atom, which shows a signal at $\delta = 156.92$ ppm, about 20 ppm downfield shifted compared to (2,6-$Mes_2C_6H_3)_2InBr$.[26]

The molecular structure of **4** is shown in Figure 3. Selected bond parameters of the series $[(2,6\text{-}Mes_2C_6H_3)_2E]^+$ (E=Al (**2**),[4] Ga (**3**),[5] In (**4**) and Tl (**5**)[6]) are collected in Table 3. The C–In-C angle is nearly linear (176.2(1)°), which is by about 20° larger than in the starting material. The value compares well with those of **3** (175.7(1)°) and **5** (177.4(3)°), but differs from that of **2** (159.2(1)°), which is attributed to the stronger intramolecular interactions between the Al atom and the flanking mesityl groups (see computational analysis below). The In–C bond lengths of **4** (2.092(2) and 2.089(2) Å) are considerably shorter than in the starting material (2.171(3) and 2.166(3) Å). In fact, they seem to be the shortest known In–C bond lengths, which usually fall in the range between 2.11 Å (Me_2InBr) and 2.24 Å ($K[InMe_4]$).[28]

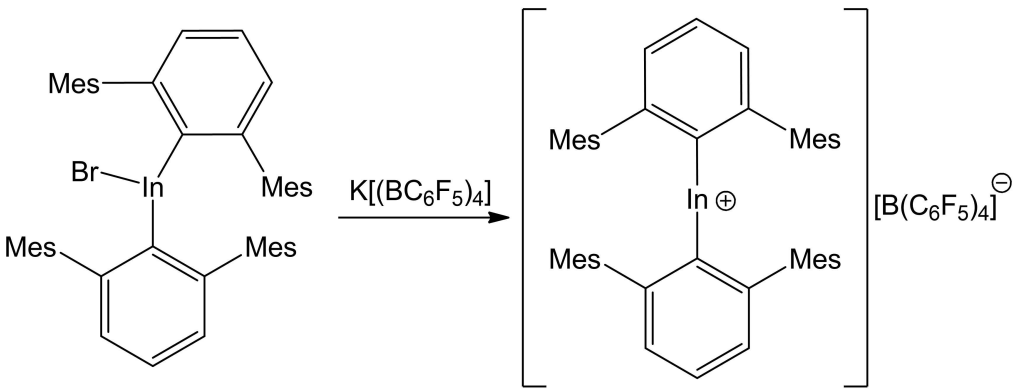

4

Scheme 2. Synthesis of the bis(*m*-terphenyl)indinium ion **4**.

Research Article
doi.org/10.1002/ejic.202200482

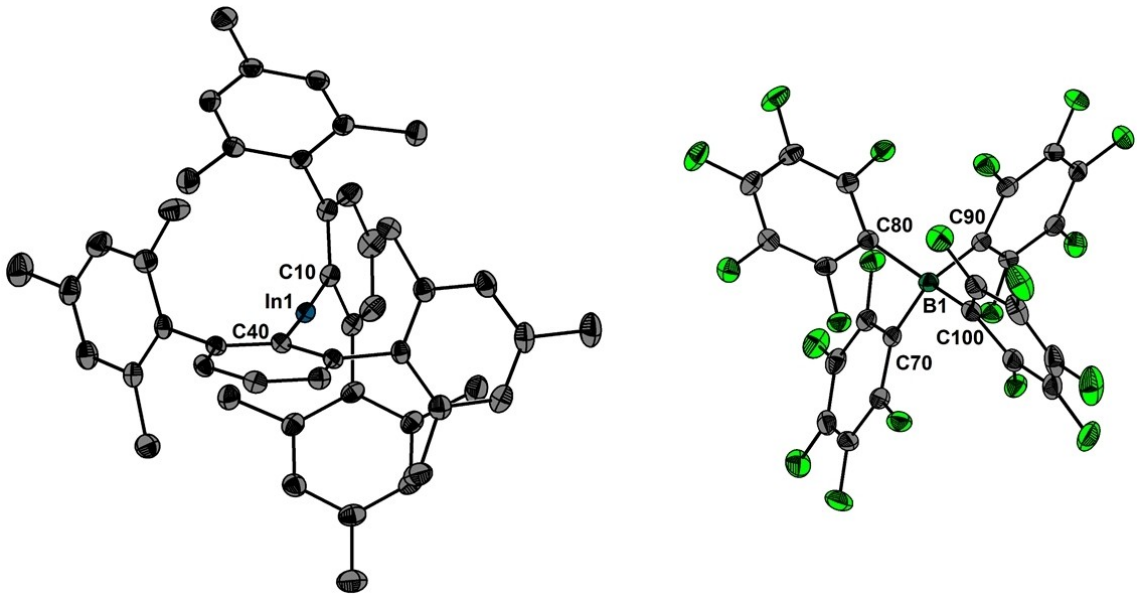

Figure 3. Molecular structure of **4** (left) and the counter anion (right) showing 50% probability ellipsoids.

Table 3. Selected bond lengths in Å and angles in ° of $[(2,6\text{-}Mes_2C_6H_3)_2E]^+$ (**2**, E=Al;[4] **3**, E=Ga;[5] **4**, E=In; **5** E=Tl[6]).

	2 (E=Al)	**3** (E=Ga)	**4** (E=In)	**5** (E=Tl)
E–C	1.938(1)	1.913(1)	2.092(2)	2.126(9)
	1.941(1)	1.915(1)	2.089(2)	2.127(9)
C–E–C	159.2(1)	175.7(1)	176.2(1)	177.4(3)

Density functional theory (DFT) and real space bond indicator (RSBI) analyses

The electronic structures in the bis(*m*-terphenyl)element cations $[(2,6\text{-}Mes_2C_6H_3)_2E]^+$ of group 13 (**1**, E=B; **2**, E=Al; **3**, E=Ga; **4**, E=In; **5**, E=Tl) were studied computationally by means of density functional theory (DFT) and real-space bonding indicator (RSBI) analysis. For this purpose, all five structures were fully optimized as isolated molecules (see ESI for details). The calculated molecular geometries match those obtained experimentally by X-ray crystallography very well. Topological and integrated bond parameters of the primary and secondary E–C interactions of **1**–**5** are collected in Table 4. AIM atomic and fragmental charges of **1**–**5** are listed in Table 5.[8] The AIM bond topology[8] as well as NCI[9] and ELI–D *iso*-surfaces[10] of **1** and **2** are shown in Figure 4 and Figure 5 (for **3**–**5**, see ESI).

The short B–C bond of **1** is dominated by covalent bonding aspects, which is reflected in a high electron density (ED, $\rho(\mathbf{r})_{bcp}$) at the bond critical point (bcp) of 1.5 eÅ^{-3}, a negative value of the Laplacian of the ED ($\nabla^2\rho(\mathbf{r})_{bcp} = -10.2$ eÅ^{-5}) and the total energy density over ED ratio also being significantly negative ($H/\rho(\mathbf{r})_{bcp} = -1.18$ a.u.). However, ionic bond contributions cannot be neglected, resulting in a considerably positive kinetic energy density over ED ratio ($G/\rho(\mathbf{r})_{bcp} = 0.71$ a.u.) and a Raub-Jansen Index (RJI)[29] of 82%, indicating that more than 80% of the electron populations of the ELI–D B–C bonding basins ($N_{ELI} = 2.78$ e) are located in the C atomic AIM basins, suggesting a perceivable bond polarity.

The longer E–C bonds of **2**–**5** (E=Al - Tl) show properties of typical polar-covalent interactions in which neither bonding

Table 4. Topological and integrated AIM and ELI–D properties of the primary E–C bonds and secondary E···C_π contacts in $[(2,6\text{-}Mes_2C_6H_3)_2E]^+$ of group 13 (**1**, E=B; **2**, E=Al; **3**, E=Ga; **4**, E=In; **5**, E=Tl).

	Contact or basin	d [Å]	$\rho(\mathbf{r})_{bcp}$ [eÅ^{-3}]	$\nabla^2\rho(\mathbf{r})_{bcp}$ [eÅ^{-5}]	ε	$G/\rho(\mathbf{r})_{bcp}$ [a.u.]	$H/(\mathbf{r})_{bcp}$ [a.u.]	N_{ELI} [e]	V_{ELI} [Å^3]	γ_{ELI}	RJI [%]
1	B–C	1.476	1.52	−10.2	0.14	0.71	−1.18	2.78	10.4	1.99	81.5
2	Al–C	1.938	0.63	6.4	0.07	1.12	−0.40	2.42	9.9	1.98	89.6
3	Ga–C	1.925	0.87	2.5	0.07	0.73	−0.52	2.61	10.7	1.68	63.0
4	In–C	2.094	0.77	2.9	0.08	0.69	−0.43	2.16	10.4	1.64	72.7
5	Tl–C	2.110	0.85	1.6	0.08	0.59	−0.46	1.84	7.0	1.56	72.7
2	Al···C_π	2.362	0.23	1.5	1.94	0.71	−0.26				
3	Ga···C_π	2.575	0.21	1.6	1.79	0.66	−0.11				

For all bonds, d is the geometric contact distance, $\rho(\mathbf{r})_{bcp}$ is the electron density at the bcp, $\nabla^2\rho(\mathbf{r})_{bcp}$ is the corresponding Laplacian, ε is the bond ellipticity, $G/\rho(\mathbf{r})_{bcp}$ and $H/\rho(\mathbf{r})_{bcp}$ are the kinetic and total energy density over $\rho(\mathbf{r})_{bcp}$ ratios, N_{ELI} and V_{ELI} are electron populations and volumes of related ELI–D basins, γ_{ELI} is the ELI–D value at the attractor position, RJI is the Raub-Jansen Index. Values are averaged over similar bonds (see Table S3 for all bonds).

Research Article
doi.org/10.1002/ejic.202200482

Table 5. AIM atomic and fragmental charges of $[(2,6\text{-}Mes_2C_6H_3)_2E]^+$ of group 13 (**1**, E=B; **2**, E=Al; **3**, E=Ga; **4**, E=In; **5**, E=Tl) in e.[a]

Q_{AIM}	R_2B^+	R_2Al^+	R_2Ga^+	R_2In^+	R_2Tl^+
R	−0.46	−0.61	−0.17	−0.12	−0.01
R′	−0.46	−0.61	−0.15	−0.12	−0.01
E	1.92	2.22	1.35	1.25	1.02
Σ	1.00	1.00	1.02	1.00	0.99

[a] R, R′ = 2,6-$Mes_2C_6H_3$.

aspect – covalent or ionic – prevails. The ED varies between 0.63 and 0.87 eÅ^{-3}, the Laplacian is positive but close to zero, and the absolute value of $G/\rho(\mathbf{r})_{bcp}$ exceeds that of $H/\rho(\mathbf{r})_{bcp}$. RJI varies between 63% in **3** and 90% in **2**. Notably, **2** and **3** (but not **1**, **4** and **5**) exhibit additional secondary E···C_π bond paths and bcps to the 2,6-$Mes_2C_6H_3$ substituents (Figure 5a and Figure S25a), which are reminiscent of similar contacts in related group 15 cations $(2,6\text{-}Mes_2C_6H_3)_2E^+$ (E=As, Sb, Bi).[12] Such kinetic stabilization via E···C_π London-dispersive/electrostatic-type interactions was not observed for the borinium or phosphenium ions, $[(2,6\text{-}Mes_2C_6H_3)_2B]^+$ or $[(2,6\text{-}Mes_2C_6H_3)_2P]^+$, both of which could not be isolated despite significant efforts. With ED values below 0.25 eÅ^{-3}, strong $G/\rho(\mathbf{r})_{bcp}$ and small negative $H/\rho(\mathbf{r})_{bcp}$ values, these Al/Ga···C_π contacts are clearly dominated by ionic bond contributions. This is supported by the NCI *iso*-surfaces, which show localized, blue-colored NCI basins for the secondary Al/Ga···C_π contacts, whereas all other weak secondary contacts, such as π···π, H···H, etc. cause the formation of extended flat, green-colored NCI basins (Figure 4b, Figure 5b and Figures S25b-S27b). (Polarized) covalent bonds do not lead to the formation of NCI basins at the commonly chosen *iso*-value of 0.5. AIM atomic and fragmental charges disclose that charge separation between group 13 element E and the *m*-terphenyl substituents increases in the order Al > B > Ga ≈ In > Tl (Table 5).

A common method to assess the relative strength of isolated Lewis acids on the basis of DFT entails the calculation of the fluoride ion affinity (FIA).[30] The FIA values calculated for the divalent bis(*m*-terphenyl)element cations $[(2,6\text{-}Mes_2C_6H_3)_2E]^+$ of group 13 (**1**, E=B; **2**, E=Al; **3**, E=Ga; **4**, E=In; **5**, E=Tl) and group 15 (**6**, E=P; **7**, E=As; **8**, E=Sb; **9**, E=Bi) are collected in Figure 6. In addition, series of calculations were conducted on small Lewis acids for comparison at three levels of theory (B3PW91, BP86, and MP2 on the structures optimized at the B3PW91 level), which are given in the ESI (Tables S6–S8). For the group 13 compounds, the FIA values fall in the rather wide range between 725 (**1**) and 520 (**5**), whereas the group 15

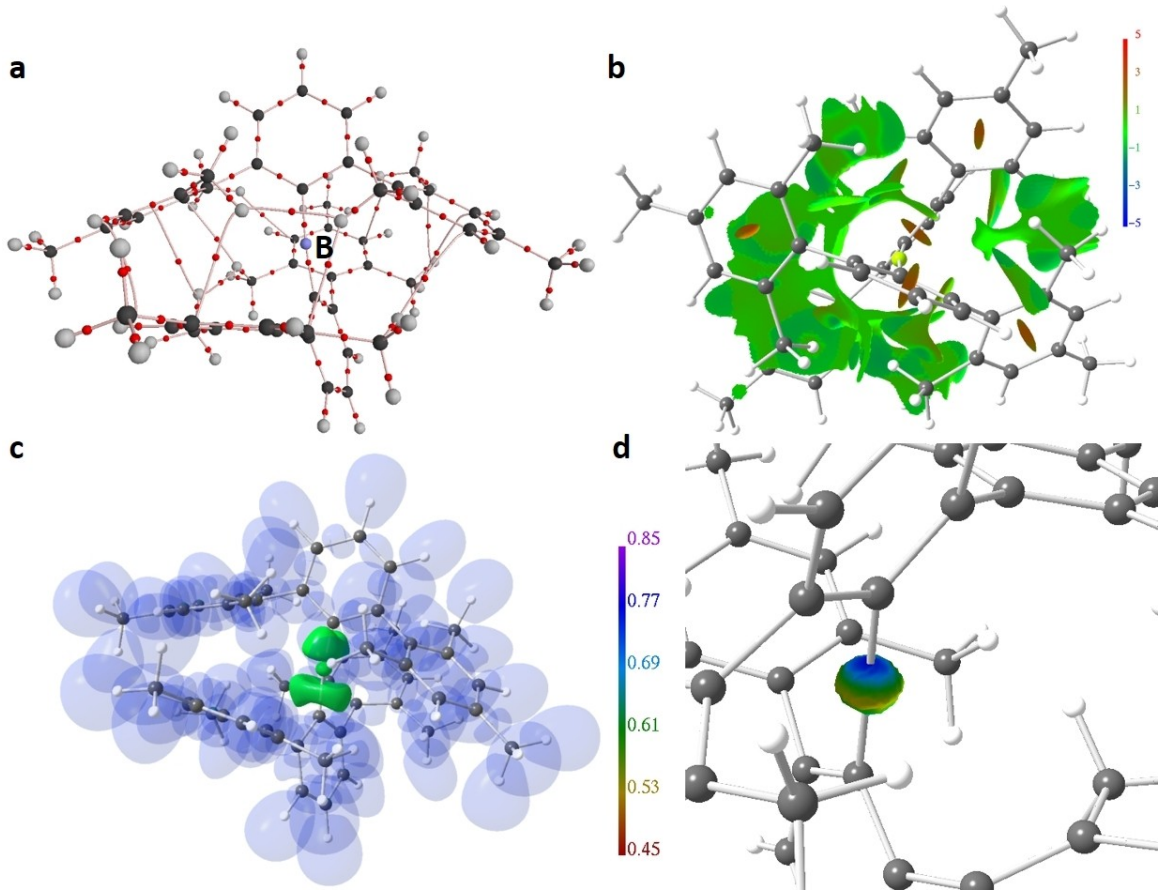

Figure 4. RSBI analysis of **1**: (a) AIM bond paths motif, (b) NCI *iso*-surface at s(**r**) = 0.5 colour coded with sign(λ_2)•ρ, (c) ELI–D localization domain representation at *iso*-value of 1.3, (d) ELI–D distribution mapped on the B atom ELI–D core basin.

Research Article
doi.org/10.1002/ejic.202200482

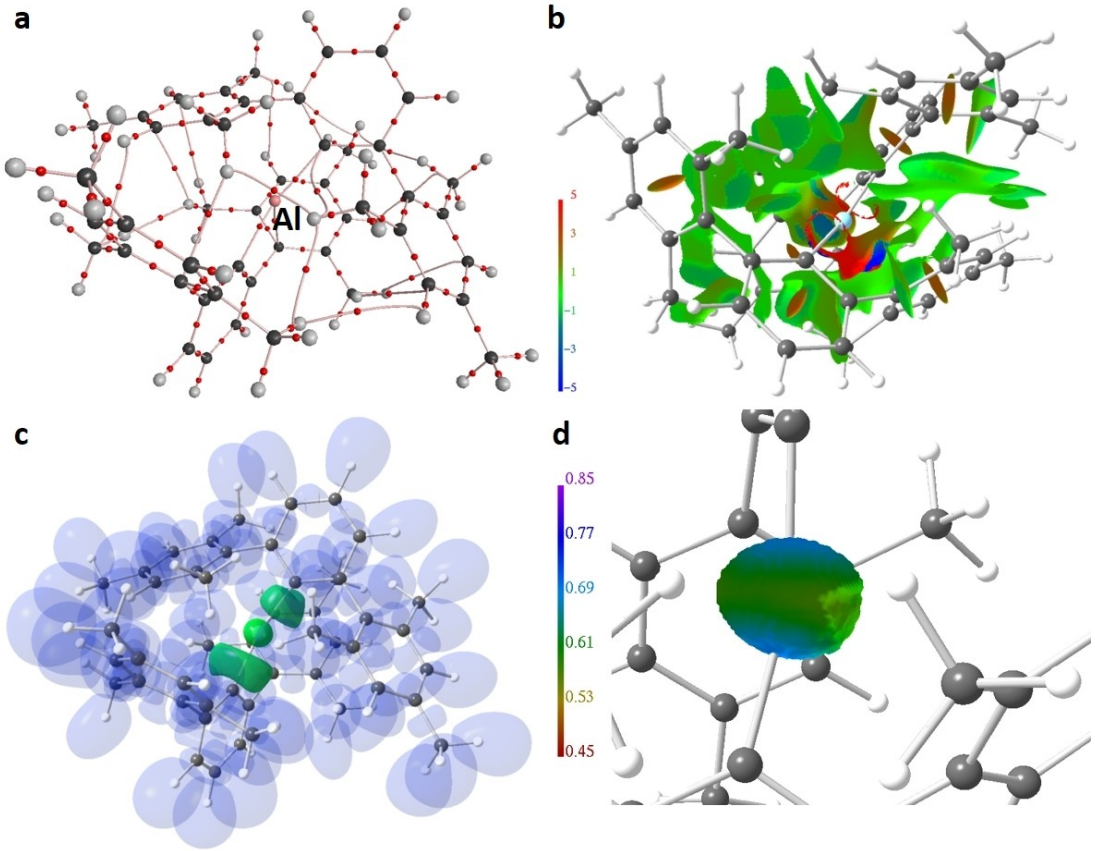

Figure 5. RSBI analysis of **2**: (a) AIM bond paths motif, (b) NCI *iso*-surface at s(**r**) = 0.5 colour coded with sign(λ_2)•ρ, (c) ELI–D localization domain representation at *iso*-value of 1.3, (d) ELI–D distribution mapped on the Al atom ELI–D core basin.

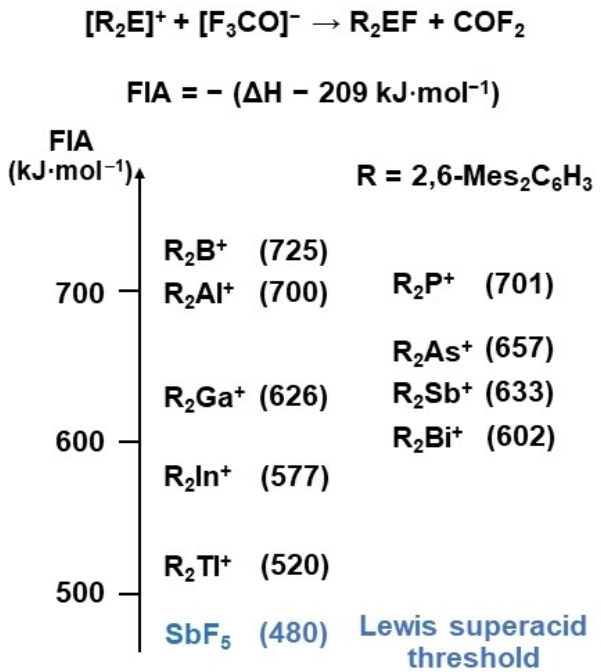

Figure 6. Calculated fluoride ion affinity (FIA) of $[(2,6\text{-}Mes_2C_6H_3)_2E]^+$ of group 13 (**1**, E=B; **2**, E=Al; **3**, E=Ga; **4**, E=In; **5**, E=Tl) and group 15 (**6**, E=P; **7**, E=As; **8**, E=Sb; **9**, E=Bi).

compounds cover the smaller range from 701 (**6**) to 602 (**9**). All of these values are smaller than those of the silyl cations $[Et_3Si]^+$ (808) and $[Mes_3Si]^+$ (778), but larger than that of SbF_5 (480), which qualifies **1**–**9** as Lewis superacids.

Conclusions

The first donor-free divalent indinium cation $[(2,6\text{-}Mes_2C_6H_3)_2In]^+$ (**4**) was obtained using sterically demanding *m*-terphenyl substituents in combination with a weakly coordinating anion, namely tetrakis(pentafluorophenyl)borate. Calculated fluoride anion affinity (FIA) qualifies **4** as Lewis superacid. Attempts to prepare the related borinium ion $[(2,6\text{-}Mes_2C_6H_3)_2B]^+$ (predicted to be an even stronger Lewis superacid) by fluoride or hydride abstraction from appropriate precursors failed on all accounts.

Experimental procedures

General information

Unless otherwise stated, all reactions and manipulations were performed under inert atmosphere (argon) using anhydrous

solvents. The starting materials 2,6-$Mes_2C_6H_3Li$ (Mes = 2,4,6-$Me_3C_6H_2$)[13] (2,6-$Mes_2C_6H_3)_2InBr$,[26] $K[B(C_6F_5)_4]$[27] $[Ph_3C][B(C_6F_5)_4]$[20] and $[Me_3Si{-}H{-}SiMe_3][B(C_6F_5)_4]$[19] were prepared following the published procedures. The reagents $BF_3{\cdot}Et_2O$, $AlCl_3$, $EtAlCl_2$ (0.9 M in hexanes), $LiAlH_4$, MeI, and $InBr_3$ were obtained commercially and were used as received. Anhydrous dichloromethane, hexane, tetrahydrofurane and toluene were collected from an SPS800 mBraun solvent purification system and stored over 4 Å molecular sieves. Et_2O was dried by refluxing it over Na/benzophenone under argon atmosphere. Deuterated solvents were degassed and dried over 4 Å molecular sieves under argon.

Unless otherwise noted, NMR spectra were recorded at room temperature on a Bruker Avance 600 MHz spectrometer. ^1H, $^{13}C\{^1H\}$, ^{11}B, $^{11}B\{^1H\}$ and ^{19}F NMR spectra are reported on the δ scale (ppm) and are referenced against $SiMe_4$. ^1H and $^{13}C\{^1H\}$ chemical shifts are reported relative to the residual peak of the solvent ($CDHCl_2$ 5.32 ppm for CD_2Cl_2, C_6D_5H for C_6D_6 and *o*-$C_6D_3HCl_2$ for *o*-$C_6D_4Cl_2$) in the ^1H NMR spectra, and to the peak of the deuterated solvent (CD_2Cl_2 53.84 ppm, C_6D_6 128.39 ppm) in the $^{13}C\{^1H\}$ NMR spectra. The assignment of the ^1H and $^{13}C\{^1H\}$ resonance signals was made in accordance with the COSY, HSQC and HMBC spectra. The labelling schemes are attached to the ^1H and ^{13}C spectra.

The ESI HRMS spectra were measured on a Bruker Impact II spectrometer. Acetonitrile or dichloromethane/acetonitrile solutions ($c = 1{\cdot}10^{-5}$ mol·L^{-1}) were injected directly into the spectrometer at a flow rate of 3 μL·min^{-1}. Nitrogen was used both as a drying gas and for nebulization with flow rates of approximately 5 L·min^{-1} and a pressure of 5 psi. Pressure in the mass analyzer region was usually about $1{\cdot}10^{-5}$ mbar. Spectra were collected for 1 min and averaged. The nozzle-skimmer voltage was adjusted individually for each measurement.

IR spectra were recorded on a *Nicolet* Thermo iS10 scientific spectrometer with a diamond ATR unit. The absorption bands are reported in cm^{-1} with indicated relative intensities: s (strong, 0–33% T); m (medium, 34–66% T), w (weak, 67–100% T), and br (broad). The UV-Vis spectra were recorded on a Varian Cary 50 Scan UV-Visible spectrophotometer.

Synthesis and characterization of $Mes_2C_6H_3BF_2$ (10). A solution of 2,6-$Mes_2C_6H_3Li$ (3.20 g, 10.0 mmol, 1.00 eq.) in Et_2O (50 mL) is added over a solution of $BF_3{\cdot}OEt_2$ (2.00 mL, 15.8 mmol, 1.58 eq.) in Et_2O (50 mL) at 0 °C over the course of 20 minutes. The reaction mixture s stirred for 2 hours at room temperature and the solvent is removed under reduced pressure. The remaining solid is extracted with DCM and filtered through a pad of celite. Afterwards the solvent is removed under vacuum and the residue washed with MeCN (3 × 10 mL) and *n*-hexane (3 × 10 mL). The remaining solid is dried under reduced pressure to obtain the title compound as a colourless solid (2.37 g, 66%).

^1H NMR (600 MHz, CD_2Cl_2): $\delta = 7.64$ (t, $^3J(^1H{-}^1H) = 7.65$ Hz, 1H, H4), 7.16 (d, $^3J(^1H{-}^1H) = 7.65$ Hz, 2H, H3 and H5), 6.97 (s, 4H, H9 and H11), 2.34 (s, 6H, H14), 2.03 (s, 12H, H13 and H15) ppm.**$^{13}C\{^1H\}$ NMR (151 MHz, CD_2Cl_2)**: $\delta = 146.94$ (s, C2 and C6), 138.85 (s, C7), 137.79 (s, C10), 136.39 (s, C8 and C12), 132.26 (s, C4), 128.59 (s, C9 and C11), 128.15 (s, C3 and C5), 21.41 (s. C14), 20.77 (s, C13 and C15) ppm. **$^{11}B\{^1H\}$ NMR (CD_2Cl_2, 193 MHz)**: $\delta = 25.32$ ppm. **$^{19}F\{^1H\}$ NMR (CD_2Cl_2, 565 MHz)**: $\delta = -70.89$ ppm. **HRMS ESI (m/z)**: $[M+F]^-$ calculated. for $C_{24}H_{25}BF_3$, 381.20069; found, 381.20086.

Synthesis and characterization of (2,6-$Mes_2C_6H_3)_2BF$ (11). A Schlenk tube is charged with **10** (1.81 g, 5.00 mmol, 1.00 eq.) and 2,6-$Mes_2C_6H_3Li$ (1.60 g, 5.00 mmol, 1.00 eq.) before *n*-hexane (40 mL) is added. The reaction mixture is stirred for 72 h and monitored by ^{19}F-NMR spectroscopy. Then the solvent is removed under reduced pressure, the residue extracted with CH_2Cl_2 (40 mL) and filtered off from any insoluble materials. The solvent is removed under vacuum and the remaining solid washed with MeCN (3 × 10 mL) and *n*-hexane (3 × 10 mL). The residual solid is dried at 80 °C/$5{\cdot}10^{-3}$ mbar to obtain **11** as off-white solid (2.98 g, 82%).

^1H NMR (600 MHz, CD_2Cl_2): $\delta = 7.22$ (t, $^3J(^1H{-}^1H) = 7.60$ Hz, 1H, H4), 6.80 (s, 4H, H9 and H11), 6.68 (d, $^3J(^1H{-}^1H) = 7.60$ Hz, 2H, H3 and H5), 2.32 (s, 6H, H14), 1.61 (s, 12H, H13 and H15) ppm. **$^{13}C\{^1H\}$ NMR (151 MHz, CD_2Cl_2)**: $\delta = 147.71$ (d, $^3J(^{13}C{-}^{19}F) = 4.70$ Hz, C2 and C6), 140.88 (s, C7), 137.45 (s, C8 and C12), 136.69 (s, C10), 130.61 (s, C3 and C5), 129.84 (s, C4), 128.66 (s, C9 and C11), 22.29 (s, C13 and C15), 21.38 (s, C14) ppm. **$^{11}B\{^1H\}$ NMR (193 MHz, CD_2Cl_2)**: $\delta = 51.48$ (s, br) ppm. **$^{19}F\{^1H\}$ NMR (565 MHz, CD_2Cl_2)**: $\delta = 17.53$ (s). **HRMS ESI (m/z)**: no signal in negative and positive mode.

Synthesis and characterization of (2,6-$Mes_2C_6H_3)_2BH$ (12). A Schlenk tube is charged with **11** (656 mg, 1.00 mmol, 1.00 eq.) and $LiAlH_4$ (80.0 mg, 2.00 mmol, 2.00 eq.) and cooled with an ice bath to 0 °C. Diethylether (12 mL) is added slowly. The reaction mixture is stirred for 48 h. Then, the solvent is removed under reduced pressure and the residue is dried at 60 °C/$5{\cdot}10^{-3}$ mbar. The remaining solid is dissolved in THF (12 mL) and to this methyl iodide (0.20 mL, 3.22 mmol, 8.46 eq.) is added. During the addition effervescence is visible. After 1 h of stirring the solvent is removed under reduced pressure and the residual solid is dried at 80 °C/$5{\cdot}10^{-3}$ mbar. Afterwards *n*-hexane (12 mL) is added and the reaction mixture is warmed up to 60 °C and the suspension is filtered. The solvent is removed under reduced pressure to yield **12** as colourless solid (613 mg, 96%).

^1H NMR (600 MHz, C_6D_6): $\delta = 6.97$ (t, $^3J(^1H{-}^1H) = 7.60$ Hz, 1H, H4), 6.87 (s, 4H, H9 and H11), 6.74 (d, $^3J(^1H{-}^1H) = 7.60$ Hz, 2H, H3 and H5), 2.19 (s, 6H, H14) 1.91 (s, 12H, H13 and H15) ppm. H6 is not visible in a range of −50 to +50 ppm, which might be due to extreme broadening and splitting of the signal. **$^{13}C\{^1H\}$ NMR (151 MHz, C_6D_6)**: $\delta = 148.59$ (s, C2 and C6), 141.40 (s, C7), 136.30 (s, C8 and C12), 135.95 (s, C10), 131.04 (s, C4), 129.50 (s, C3 and C5), 128.83 (s, C9 and C11), 22.90 (s, C13 and C15), 21.21 (s, C14) ppm. **^{11}B NMR (193 MHz, C_6D_6)**: $\delta = 74.27$ (s, br) ppm. **HRMS ESI (m/z)**: no signal in negative and positive mode. **IR (ATR, neat)**: (B–H) = 2580 (m) cm^{-1}.

Attempted Synthesis of [(2,6-$Mes_2C_6H_3)_2B$][$B(C_6F_5)_4$] from [$Me_3SiHSiMe_3$][$B(C_6F_5)_4$]. A Schlenk tube is charged with **11** (65.6 mg, 0.10 mmol, 1.00 eq.) and [$Me_3SiHSiMe_3$][$B(C_6F_5)_4$] (82.6 mg, 0.10 mmol, 1.00 eq.) and cooled with an ice bath to 0 °C. Then, CH_2Cl_2 (4 mL) is slowly added to the solids. The solution is stirred for an hour and monitored by ^{19}F- and ^{11}B

Research Article
doi.org/10.1002/ejic.202200482

NMR spectroscopy. The solution is carefully layered with *n*-hexane (20 mL) to allow slow diffusion. The product **12** is obtained as a colourless crystalline solid (53.4 mg, 84%). The remaining oil is identified by means of ^{29}Si and ^{19}F NMR spectra as $[Me_3SiFSiMe_3][B(C_6F_5)_4]$.[18]

^{1}H NMR (600 MHz, C_6D_6): $\delta = 6.97$ (t, $^3J(^1H^{-1}H) = 7.60$ Hz, 1H, H4), 6.87 (s, 4H, H9 and H11), 6.74 (d, $^3J(^1H^{-1}H) = 7.60$ Hz, 2H, H3 and H5), 2.19 (s, 6H, H14) 1.91 (s, 12H, H13 and H15) ppm. H6 is not visible in a range of −50 to +50 ppm, which might be due to extreme broadening and splitting of the signal. **^{13}C{^{1}H} NMR (151 MHz, C_6D_6)**: $\delta = 148.59$ (s, C2 and C6), 141.40 (s, C7), 136.30 (s, C8 and C12), 135.95 (s, C10), 131.04 (s, C4), 129.50 (s, C3 and C5), 128.83 (s, C9 and C11), 22.90 (s, C13 and C15), 21.21 (s, C14) ppm. **^{11}B NMR (193 MHz, C_6D_6)**: $\delta = 74.27$ (s, br) ppm. **HRMS ESI (m/z)**: no signal in negative and positive mode. **IR (ATR, neat)**: $\tilde{\nu}$(B–H) = 2580 (m) cm^{-1}.

Attempted Synthesis of $[(Mes_2C_6H_3)_2B][B(C_6F_5)_4]$ from $[Me_3Si\cdot toluene][B(C_6F_5)_4]$ and $(Mes_2C_6H_3)_2BF$. $[Me_3SiHSiMe_3][B(C_6F_5)_4]$ (82.6 mg, 0.10 mmol, 1.00 eq.) is placed in a Schlenk tube. To this, toluene (2 mL) is added. After 2 hours the solvent of the suspension is removed under reduced pressure and (2,6-$Mes_2C_6H_3)_2BF$ (65.6 mg, 0.10 mmol, 1.00 eq.) is added. To this, 1,2-difluorobenzene (4 mL) is added and the reaction mixture is stirred for 18 hours at room temperature, leading to a dark brown solution. The solution is layered with *n*-hexane (20 mL). After complete diffusion the solvent is removed by decantation and the remaining solid is dried under reduced pressure. NMR spectra are measured in CD_2Cl_2.

^{1}H NMR (600 MHz, CD_2Cl_2): $\delta = 7.71$ (m), 7.62 (m), 7.49 (t, $^3J(^1H^{-1}H) = 7.58$ Hz, 2H), 7.16 (m), 7.12 (dd, $^3J(^1H^{-1}H) = 7.58$ Hz, $^4J(^1H^{-1}H) = 1.54$ Hz, 4H)*, 7.05 (s), 6.89 (s), 6.87 (s), 6.95 (s, 5H)*, 6.91 (t, $^4J(^1H^{-1}H) = 1.54$ Hz, 1H)*, 4.69 (s), 4.65 (s), 2.34 (s, 3H), 2.33 (s, 9H), 2.06 (s, 18H)*, 2.03 (m, 6H)* ppm. All signals marked with * are assigned to 2,6-$Mes_2C_6H_4$.

^{11}B{^{1}H} NMR (193 MHz, CD_2Cl_2): $\delta = 54.57$ (s), 41.10 (s), 28.39 (s), 25.90 (s), −16.63 (s) ppm.

Attempted Synthesis of $[(2,6\text{-}Mes_2C_6H_3)_2B][B(C_6F_5)_4]$ from $[Ph_3C][B(C_6F_5)_4]$ and $(Mes_2C_6H_3)_2BH$ (12). A Young NMR tube is charged with **12** (6.4 mg, 0.01 mmol, 1.00 eq.) and $[Ph_3C][B(C_6F_5)_4]$ (9.2 mg, 0.01 mmol, 1.00 eq.) and 1,2-$Cl_2C_6D_4$ (0.5 mL) is added. The reaction is monitored by means of ^{1}H-, ^{11}B- and ^{11}B-{^{1}H}-NMR spectroscopy. At room temperature and 60 degrees no reaction occurred. By heating to 80 °C over the course of 12 hours the starting material got completely consumed by means of ^{11}B-NMR spectroscopy and the solution turned deep brown. The ^{1}H-NMR spectrum reveals multiple $Mes_2C_6H_3$ species.

^{1}H NMR (600 MHz, $C_6D_4Cl_2$): $\delta = .7.84$ (t (br), 2H), 7.49 (t (br), 4H), 7.40 (t (br), 1H), 7.34 (s, 2H), 7.33 (s, 2H), 7.12 (t (br), 1H), 7.05 (d (br), 2H), 7.02 (d (br), 2H), 6.81 (s, 4H), 6.72 (s, 1H), 2.24 (s, 10H), 2.02 (s, 16H) ppm. Due to broadness of the signals no coupling constants could be measured. For Integration, the signal with the lowest integral in the aromatic region was chosen and set to an Integral of ^{1}H. **^{11}B{^{1}H} NMR (193 MHz, CD_2Cl_2)**: $\delta = -16.19$ ($B(C_6F_4)^-$) ppm. No further signal in the range of +200 to −200 ppm visible.

Attempted Synthesis of $[(2,6\text{-}Mes_2C_6H_3)_2B][AlCl_4]$ from $(2,6\text{-}Mes_2C_6H_3)_2BF$ (11). A Schlenk tube is charged with **12** (65.6 mg, 0.10 mmol, 1.00 eq.) and $AlCl_3$ (133 mg, 1.00 mmol, 10.0 eq.). Then, CH_2Cl_2 (4 mL) is added. After stirring for 18 hours at room temperature, a dark red solution is obtained. The solution is layered with *n*-hexane (20 mL). After complete diffusion $Mes_2C_6H_3BCl_2$ (**13**) is obtained as a crystalline solid (19.2 mg, 48%). The analytical data is according to the literature.[14]

Any attempts to isolate the corresponding aluminium compound led to a mixture of undefined and insoluble products.

Attempted Synthesis of $[(2,6\text{-}Mes_2C_6H_3)_2B][EtAlCl_3]$. A Schlenk tube is charged with 12 (118 mg, 0.18 mmol, 1.00 eq.). Then, CH_2Cl_2 (4 mL) is added. The solution is cooled down to –78 °C and $EtAlCl_2$ (2.0 mL, 1.80 mmol, 10.0 eq.) is added. After stirring for 18 hours at room temperature, a dark brown solution is obtained. The solvent is removed under reduced pressure and the residue is washed several times with *n*-hexane to remove excess $EtAlCl_2$. The remaining solid is dissolved in CH_2Cl_2 (4 mL) crashed out by addition of *n*-hexane (20 mL). The solvent is decanted of and the residue is dried under reduced pressure to obtain a dark brown oil which was analysed by NMR spectroscopy in CD_2Cl_2.

All attempts to grow crystals suitable for X-ray diffraction measurements from the different solvents (CH_2Cl_2/*n*-hexane, 1,2-difluorobenzene/*n*-hexane, hot toluene, CH_2Cl_2/toluene) failed.

Synthesis and characterization of $[(Mes_2C_6H_3)_2In][B(C_6F_5)_4]$ (4). A Schlenk tube is charged with (2,6-$Mes_2C_6H_3)_2InBr$ (82.0 mg, 0.10 mmol, 1.00 eq.) and $K[B(C_6F_5)_4]$ (71.8 mg, 0.10 mmol, 1.00 eq.). Then, CH_2Cl_2 (4 mL) is added. After stirring for 30 minutes at 20 °C the solution is layered with *n*-hexane (20 mL). After complete diffusion the solvent is removed by decantation and the remaining solid is dried under reduced pressure to yield 4 as orange crystalline solid (129 mg, 91%).

^{1}H NMR (600 MHz, CD_2Cl_2): $\delta = 7.61$ (t, $^3J(^1H^{-1}H) = 7.59$ Hz, 1H, H4), 7.25 (d, $^3J(^1H^{-1}H) = 7.59$ Hz, 2H, H3 and H5), 7.06 (s, 4H, H9 and H11), 2.30 (s, 6H, H14), 1.73 (s, 12H, H13 and H15) ppm. **^{13}C{^{1}H} NMR (151 MHz, CD_2Cl_2)**: $\delta = 156.92$ (s, C1), 147.49 (s, C2 and C6), 140.95 (s, C10), 139.92 (s, C7), 136.56 (s, C8 and C12), 134.01 (s, C4), 130.90 (s, C9 and C11), 129.16 (s, C3 and C5), 21.53 (s, C13 and C15), 21.40 (s, C14) ppm. **^{11}B{^{1}H} NMR (193 MHz, CD_2Cl_2)**: δ =-16.65 (s) ppm. **^{19}F NMR (565 MHz, CD_2Cl_2)**: $\delta = -133.39$ (s), −163.76 (t, $^3J(^{19}F^{-19}F) = 20.37$ Hz), −167.59 (t, $^3J(^{19}F^{-19}F) = 17.77$ Hz) ppm. **HRMS ESI (m/z)**: $[M]^+$ calculated. for $C_{48}H_{50}In$, 741.29458; found, 741.29441. **UV-VIS (DCM, 100 μM)**: λ(abs) = 435 nm.

X-ray diffraction studies

Single crystals of **4**, **10** and **13** were grown by slow diffusion of n-hexane into CH_2Cl_2 solutions. Single crystals of **11** and **12** were grown by crystallization from hot *n*-hexane. Single crystal X-ray diffraction data were collected at 100 K using an open flow nitrogen stream on a Bruker Venture D8 diffractometer

with a Photon 100 detector in shutterless mode using a microfocus source (Mo$K\alpha$ = 0.71073 Å). All structures were solved using the dual-space algorithm in ShelXT[31] and refined against F^2 with the use of SHELXL[31] (Independent Atom Model – IAM) within the WinGX[32] and OLEX2[33] program package. All non-hydrogen atoms were refined using anisotropic displacement parameters. Hydrogen atoms were located from the Fourier difference map and had their positions and isotropic displacement parameter refined freely. Crystal and refinement data are collected in Table S1.

The geometry of **12** obtained from the IAM provided the initial model used as input for a subsequent Hirshfeld Atom Refinement (HAR)[22] performed using the Gaussian-HAR method with the lamaGOET[34] interface at the B3LYP/def2-TZVP level of theory. A surrounding self-consistent cluster charge field of 8 Å radius around the central formula unit was used in the iterative quantum chemical calculation step in order to simulate the crystal environment influence over the theoretical electron densities. HAR was performed against F using a merged set of reflections, whereby negative $|F|^2$ reflections, $|F| < 4.0$ sigma($|F|$) and all systematic absences were pruned. All H atoms were refined freely and anisotropically within HAR. Ortep-type figures were created using DIAMOND.[35]

Deposition Numbers 2177924 (for **4**), 2177925 (for **10**), 2177926 (for **11**), 2177927 (for **12**), and 2177928 (for **13**) contain the supplementary crystallographic data for this paper. These data are provided free of charge by the joint Cambridge Crystallographic Data Centre and Fachinformationszentrum Karlsruhe Access Structures service www.ccdc.cam.ac.uk/structures.

Computational studies

Starting from the solid-state molecular geometries density functional theory (DFT) computations were performed in the gas-phase at the B3PW91/6-311 + G(2df,p)[36] level of theory using Gaussian09.[37] For the In and Tl atoms, effective core potentials (ECP28MDF, ECP60MDF)[38] and corresponding cc-pVTZ basis set[38] were utilized. Dispersion was taken account for by the empirical dispersion correction of Grimme.[39] Subsequent normal mode analysis had to be skipped as it exceeded computational capacities. The wavefunction files were used for a topological analysis of the electron density according to the Atoms-In-Molecules space-partitioning scheme[8] using AIM2000,[40] whereas DGRID[41] was used to generate and analyze the Electron-Localizability-Indicator (ELI–D)[10] related real-space bonding descriptors applying a grid step size of 0.05 a.u. (0.12 a.u. for visualization). The NCI[9] grids were computed with NCIplot (0.1 a.u. grids).[42] Bond paths are displayed with AIM2000, ELI–D and NCI figures are displayed with MolIso,[43] AIM provides a bond paths motif, which resembles and exceeds the Lewis picture of chemical bonding, disclosing all types and strengths of interactions. Additionally, it provides atomic volumes and charges. Analyses of the reduced density gradient, $s(\mathbf{r}) = [1/2(3\pi^2)^{1/3}]|\nabla\rho|/\rho^{4/3}$, according to the NCI method is used to visualize non-covalent bonding aspects. An estimation of different non-covalent contact types according to steric/repulsive ($\lambda_2 > 0$), van der Waals-like ($\lambda_2 \approx 0$), and attractive ($\lambda_2 < 0$) is facilitated by mapping the ED times the sign of the second eigenvalue of the Hessian ($\mathrm{sign}(\lambda_2)\rho$) on the *iso*-surfaces of $s(\mathbf{r})$. AIM and NCI are complemented by the ELI–D, which provides electron populations and volumes of bonding and lone-pair basins and is especially suitable for the analysis of (polar-)covalent bonding aspects.

Acknowledgements

The Deutsche Forschungsgemeinschaft (DFG) is gratefully acknowledged for financial support. Open Access funding enabled and organized by Projekt DEAL.

Conflict of Interest

The authors declare no conflict of interest.

Data Availability Statement

The data that support the findings of this study are available from the corresponding author upon reasonable request.

Keywords: Boron · Indium · Indinium cations · Lewis acids · Superacids

[1] a) W. E. Piers, S. C. Bourke, K. D. Conroy, *Angew. Chem. Int. Ed.* **2005**, *44*, 5016–5036; *Angew. Chem.* **2005**, *117*, 5142–5163; b) X. Tan, H. Wang, *Chem. Soc. Rev.* **2022**, *51*, 2583–2600.
[2] S. Dagorne, D. A. Atwood, *Chem. Rev.* **2008**, *108*, 4037–4071.
[3] Y. Shoji, N. Tanaka, K. Mikami, M. Uchiyama, T. Fukushima, *Nat. Chem.* **2014**, *6*, 498–503.
[4] J. D. Young, M. A. Khan, R. J. Wehmschulte, *Organometallics* **2004**, *23*, 1965–1967.
[5] R. J. Wehmschulte, J. M. Steele, J. D. Young, M. A. Khan, *J. Am. Chem. Soc.* **2003**, *125*, 1470–1471.
[6] S. U. Ahmad, J. Beckmann, *Organometallics* **2009**, *28*, 6893–6901.
[7] a) I. Peckermann, D. Robert, U. Englert, T. P. Spaniol, J. Okuda, *Organometallics* **2008**, *27*, 4817–4820; b) F. Gahlmann, B. Neumüller, *Z. Anorg. Allg. Chem.* **1994**, *620*, 847–850.
[8] R. W. F. Bader, *Atoms in Molecules: A Quantum Theory* (Cambridge University Press: Oxford U. K., **1991**).
[9] E. R. Johnson, S. Keinan, P. Mori-Sanchez, J. Contreras-García, A. J. Cohen, W. Yang, *J. Am. Chem. Soc.* **2010**, *132*, 6498–6506.
[10] M. Kohout, F. R. Wagner, Y. Grin, *Theor. Chem. Acc.* **2008**, *119*, 413–420.
[11] M. Olaru, D. Duvinage, E. Lork, S. Mebs, J. Beckmann, *Chem. Eur. J.* **2019**, *25*, 14758–14761.
[12] M. Olaru, D. Duvinage, S. Mebs, J. Beckmann, *Angew. Chem. Int. Ed.* **2018**, *57*, 10080–10084; *Angew. Chem.* **2018**, *130*, 10237–10241.
[13] K. Ruhlandt-Senge, J. J. Ellison, R. J. Wehmschulte, F. Pauer, P. P. Power, *J. Am. Chem. Soc.* **1993**, *115*, 11353–11357.
[14] W. J. Gribsy, P. P. Power, *J. Am. Chem. Soc.* **1996**, *118*, 7981–7988.
[15] a) A. G. Massey, A. J. Park, *J. Organomet. Chem.* **1964**, *2*, 245–250; b) M. Kuprat, M. Lehmann, A. Schulz, A. Villinger, *Organometallics* **2010**, *29*, 1421–1427.
[16] J. F. Kögel, A. Y. Timoshkin, A. Schröder, E. Lork, J. Beckmann, *Chem. Sci.* **2018**, *9*, 8178–8183.
[17] J. B. Lambert, S. Zhang, S. M. Ciro, *Organometallics* **1994**, *13*, 2430–2443.

[18] M. Lehmann, A. Schulz, A. Villinger, *Angew. Chem. Int. Ed.* **2009**, *48*, 7444–7447; *Angew. Chem.* **2009**, *121*, 7580–7583.
[19] R. J. Wehmschulte, A. A. Diaz, M. A. Kahn, *Organometallics* **2003**, *22*, 83–92.
[20] J. C. W. Chien, W.-M. Tsai, M. D. Rausch, *J. Am. Chem. Soc.* **1991**, *113*, 8570–8571.
[21] S. M. Cornet, K. B. Dillon, C. D. Entwistle, M. A. Fox, A. E. Goeta, H. P. Goodwin, T. B. Marder, A. L. Thompson, *Dalton Trans.* **2003**, 4395–4405.
[22] a) D. Jayatilaka, B. Dittrich, *Acta Crystallogr.* **2008**, *A64*, 383–393; b) S. C. Capelli, H.-B. Bürgi, B. Dittrich, S. Grabowsky, D. Jayatilaka, *IUCrJ* **2014**, *1*, 361–379.
[23] M. Woińska, S. Grabowsky, P. M. Dominiak, K. Woźniak, D. Jayatilaka, *Sci. Adv.* **2016**, *2*, e1600192.
[24] F. Kleemiss, O. V. Dolomanov, M. Bodensteiner, N. Peyerimhoff, L. Midgley, L. J. Bourhis, A. Genoni, L. A. Malaspina, D. Jayatilaka, J. L. Spencer, F. White, B. Grundkötter-Stock, S. Steinhauer, D. Lentz, H. Puschmann, S. Grabowsky, *Chem. Sci.* **2021**, *12*, 1675–1692.
[25] E. Damgaard-Møller, L. Krause, H. Lassen, L. A. Malaspina, S. Grabowsky, H. Bamberger, J. McGuire, H. N. Miras, S. Sproules, J. Overgaard, *Inorg. Chem.* **2020**, *59*, 13190–13200.
[26] X.-W. Li, G. H. Robinson, W. T. Pennington, *Main Group Chem.* **1996**, *1*, 301–307.
[27] P. Romanato, S. Duttwyler, A. Linden, K. K. Baldridge, J. S. Siegel, *J. Am. Chem. Soc.* **2010**, *132*, 7828–7829.
[28] a) H. D. Hausen, K. Mertz, J. Weidlein, W. Schwarz, *J. Organomet. Chem.* **1975**, *93*, 291–296; b) K. Hoffmann, E. Weiss, *J. Organomet. Chem.* **1973**, *50*, 17–24; c) B. Cordero, V. Gómez, A. E. Platero-Prats, M. Revés, J. Echeverria, E. Cremades, F. Barragán, S. Alvarez, *Dalton Trans.* **2008**, *21*, 2832–2838.
[29] S. Raub, G. A. Jansen, *Theor. Chem. Acc.* **2001**, *106*, 223–232.
[30] P. Erdmann, J. Leitner, J. Schwarz, L. Greb, *ChemPhysChem* **2020**, *21*, 987–994.
[31] G. M. Sheldrick, *Acta Crystallogr.* **2015**, *C71*, 3–8.
[32] L. J. Farrugia, *J. Appl. Crystallogr.* **2012**, *45*, 849–854.
[33] O. V. Dolomanov, L. J. Bourhis, R. J. Gildea, J. A. Howard, H. Puschmann, *J. Appl. Crystallogr.* **2009**, *42*, 339–341.
[34] L. A. Malaspina, A. Genoni, S. Grabowsky, *J. Appl. Crystallogr.* **2021**, *54*, 987–995.
[35] K. Brandenburg, Diamond, Version 4.0.4, Crystal Impact GbR: Bonn, Germany, **2012**.
[36] a) A. D. Becke, *J. Chem. Phys.* **1993**, *98*, 5648–5652; b) J. P. Perdew, J. A. Chevary, S. H. Vosko, K. A. Jackson, M. R. Pederson, D. J. Singh, C. Fiolhais, *Phys. Rev.* B **1992**, *46*, 6671–6687.
[37] M. J. Frisch, G. W. Trucks, H. B. Schlegel, G. E. Scuseria, M. A. Robb, J. R. Cheeseman, G. Scalmani, V. Barone, G. A. Petersson, H. Nakatsuji, X. Li, M. Caricato, A. V. Marenich, J. Bloino, B. G. Janesko, R. Gomperts, B. Mennucci, H. P. Hratchian, J. V. Ortiz, A. F. Izmaylov, J. L. Sonnenberg, D. Williams-Young, F. Ding, F. Lipparini, F. Egidi, J. Goings, B. Peng, A. Petrone, T. Henderson, D. Ranasinghe, V. G. Zakrzewski, J. Gao, N. Rega, G. Zheng, W. Liang, M. Hada, M. Ehara, K. Toyota, R. Fukuda, J. Hasegawa, M. Ishida, T. Nakajima, Y. Honda, O. Kitao, H. Nakai, T. Vreven, K. Throssell, J. A. Montgomery, Jr., J. E. Peralta, F. Ogliaro, M. J. Bearpark, J. J. Heyd, E. N. Brothers, K. N. Kudin, V. N. Staroverov, T. A. Keith, R. Kobayashi, J. Normand, K. Raghavachari, A. P. Rendell, J. C. Burant, S. S. Iyengar, J. Tomasi, M. Cossi, J. M. Millam, M. Klene, C. Adamo, R. Cammi, J. W. Ochterski, R. L. Martin, K. Morokuma, O. Farkas, J. B. Foresman, D. J. Fox, Gaussian, Inc., Wallingford CT, **2016**.
[38] a) K. A. Peterson, *J. Chem. Phys.* **2003**, *119*, 11099; b) K. A. Peterson, D. Figgen, E. Goll, H. Stoll, M. Dolg, *J. Chem. Phys.* **2003**, *119*, 11113–11123.
[39] S. Grimme, J. Anthony, S. Ehrlich, H. Krieg, *J. Chem. Phys.* **2010**, *132*, 154104.
[40] F. Biegler-König, J. Schönbohm, D. Bayles, *J. Comput. Chem.* **2001**, *22*, 545–559.
[41] M. Kohout, *DGRID*-4.6 Radebeul, **2015**.
[42] J. Contreras-García, E. Johnson, S. Keinan, R. Chaudret, J.-P. Piquemal, D. Beratan, W. Yang, *J. Chem. Theory Comput.* **2011**, *7*, 625–632.
[43] C. B. Hübschle, P. Luger, *J. Appl. Crystallogr.* **2006**, *39*, 901–904.

Manuscript received: July 27, 2022
Revised manuscript received: August 17, 2022
Accepted manuscript online: August 19, 2022

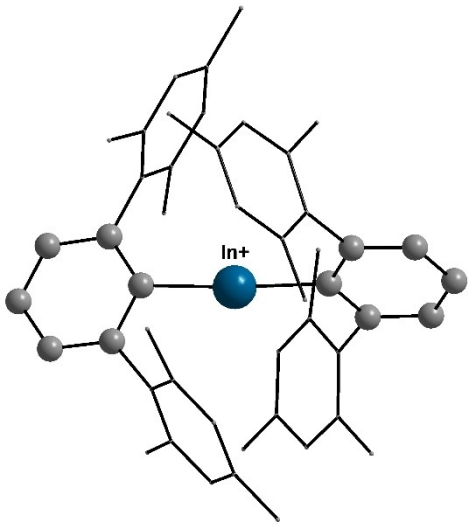

D. Duvinage, Dr. L. A. Malaspina, PD Dr. S. Grabowsky, Dr. S. Mebs*, Prof. Dr. J. Beckmann**

1 – 12

Lewis Superacidic Divalent Bis(*m*-terphenyl)element Cations [(2,6-$Mes_2C_6H_3)_2E]^+$ of Group 13 Revisited and Extended (E═B, Al, Ga, In, Tl)

The first two-coordinate diarylindinium cation $[2,6\text{-}Mes_2C_6H_3)_2In]^+$ was prepared and fully characterized.